Study of phase stability in NiPt systems

2003 J. Phys.: Condens. Matter 15 1029

(http://iopscience.iop.org/0953-8984/15/7/302)

INSTITUTE OF PHYSICS PUBLISHING JOURNAL OF PHYSICS: CONDENSED MATTER

J. Phys.: Condens. Matter **15** (2003) 1029–1046 PII: S0953-8984(03)53367-7

Study of phase stability in NiPt systems

Durga Paudyal, Tanusri Saha-Dasgupta and Abhijit Mookerjee

SN Bose National Centre for Basic Sciences, JD Block, Sector 3, Salt Lake City, Kolkata 700098, India

E-mail: dpaudyal@bose.res.in, tanusri@bose.res.in and abhijit@bose.res.in

Received 12 September 2002, in final form 12 December 2002
Published 10 February 2003
Online at stacks.iop.org/JPhysCM/15/1029

Abstract

We have studied the problem of phase stability in NiPt alloy systems. We have used the augmented space recursion based on the tight binding-linearized muffin-tin orbital as the method for studying the electronic structure of the alloys. In particular, we have used the relativistic generalization of our earlier technique. We note that, in order to predict the proper ground state structures and energetics, in addition to relativistic effects, we have to take into account charge transfer effects with precision.

1. Introduction

There has been growing interest in the study of alloy phase ordering and segregation using first-principles techniques. In order to study these phenomena one needs a derivation of the configurational energy for the alloy system. Different models have been proposed in which the configurational energies are expressed in terms of effective multi-site interactions, in particular effective pair interactions [1]. The analysis of alloy ordering tendencies and phase stability reduces to the accurate and reliable determination of effective pair interactions. There are two different approaches for obtaining effective pair interactions. One approach is to start with electronic structure calculations of the total energy of ordered super-structures of the alloy and to invert these total energies to obtain the effective pair interactions. This is the Connolly–Williams method [2]. The other approach is to start from the completely disordered phase, set up a perturbation in the form of concentration fluctuations associated with an ordered phase and study whether the alloy can sustain such a perturbation. This includes approaches like the generalized perturbation method (GPM) [3] and the embedded cluster method (ECM) [4]. Most of the works on electronic structure of the disordered alloys have been based so far on the coherent potential approximation (CPA). The CPA, being a single-site approximation, cannot take into account the effect at a site of its immediate environment. In an attempt to go beyond the single-site approximation, de Fontaine and his group followed a different approach of direct configurational averaging (DCA) [5], without resorting to any kind of single-site approximation. The effective pair and multi-site interactions were calculated directly in real

space for given configurations and the averaging was done in a brute force way by summing over different configurations. Invariably, the number of configurations was finite and convergence of the results with increasing numbers of configurations is yet to be available.

Saha *et al* [6] have introduced the augmented space recursion (ASR) based on the augmented space formalism (ASF) first suggested by Mookerjee [7] coupled with the recursion method of Haydock *et al* [8]. Within ASF the configuration averaging is carried out without having to resort to any single-site approximation. The recursion method allows us to take into account the effect of the environment of a given site. Moreover, the convergence of various physical quantities calculated through recursion with the number of recursion steps and subsequent termination has been studied in great detail [9]. Among the advantages of the ASR in going beyond the single-site approximation is the possibility of inclusion of local lattice distortions, which is important in the case of alloys with a large size mismatch between components, as in the case of NiPt. In an earlier paper Saha and Mookerjee [10] had discussed the effect of local lattice distortion on the electronic structures of CuPd and CuBe alloys using the ASR. This allows the structure matrices to randomly take values $S^{AA}_{LL'}$, $S^{AB}_{LL'}$, $S^{BA}_{LL'}$ or $S^{BB}_{LL'}$, depending on the occupation of the sites R and R'. The ASR, coupled with the orbital peeling technique [11] to evaluate small energy differences associated with band structure energies, has been successfully used in the past to describe the phase formation in alloys [12].

In the present paper we focus on the application of this method for a phase stability study in NiPt alloys. This system of alloys is of importance because of the possible need for relativistic corrections due to the heavy mass of Pt as well as effects due to charge transfer and a size mismatch between Ni and Pt. This therefore forms a perfect candidate for testing the applicability and limitations of our formalism, bringing in the relative importance of various effects for the accurate description of the system. The previous studies of ordered and substitutionally disordered NiPt alloy systems have shown the importance of the inclusion of relativistic effects. Treglia and Ducastelle [13] had shown that late transition metal alloys should exhibit phase separating tendencies but they argue that the exceptional ordering behaviour of NiPt is due to the relativistic corrections. In a first-principles study, Pinski *et al* [14] found that the disordered fcc $Ni_{1-x}Pt_x$ alloy at $x = 0.5$, calculated by means of the single-site KKR-CPA, becomes unstable at low temperatures, due to a perturbation by a $\langle 100 \rangle$ ordering wave and concluded that the corresponding long-range ordered (LRO) state, i.e. the $L1_0$ structure, should be the predicted ground state for which the large size mismatch between Ni and Pt plays the main role and the effect of relativity can be neglected. However, Lu *et al* [15] pointed out that a local ordering tendency determined by perturbation analysis does not necessarily predict the correct LRO ground state if the size mismatch of the two elements is large, as is the case for Ni and Pt, and concluded that relativity is the sole reason for long-range order in NiPt. The work of Singh *et al* [16] demonstrated that the relativistic effects do stabilize the ordered structures over the disordered solid solution. Recently Ruban *et al* [17] have studied the problem of phase stability in NiPt alloy systems based on ordered calculations with the inclusion of the Madelung energy with multipole corrections. In this paper, we examine the relativistic treatment of the Hamiltonian and charge transfer and lattice relaxation effects on the electronic structure and phase stability of face-centred cubic NiPt systems at 25, 50 and 75% of concentration of Pt. As mentioned already, the ASR technique, which we use here, is capable of taking into account environmental effects, effects of short-range order and local lattice relaxation effects due to size mismatches. To circumvent the problem of the calculation of the Madelung energy contribution for the disordered system, we have used the appropriate effective atomic sphere radii for each of the constituents so that the spheres are neutral on average and this has been done with precision at each concentration [18]. We have shown that without the inclusion of relativistic effects the formation energy comes out

to be positive, which contradicts experimental results. With the scalar relativistic corrections, involving mass–velocity and Darwin terms, the formation energy comes out to be negative, indicating that the relativistic effects play an important role in NiPt alloys, in agreement with earlier studies. We find that the charge transfer effects also have an important role to play in deciding on the correct ground state structure, particularly when the concentration of Pt is high. Our study of transition temperatures based on a mean field theory could reproduce the qualitative experimental trends.

2. Formalism

2.1. The effective pair interactions

We start from a completely disordered alloy. Each site R has an occupation variable n_R associated with it. For a homogeneous perfect disorder $\langle n_R \rangle = x$, where x is the concentration of one of the components of the alloy. In this homogeneously disordered system we now introduce fluctuations in the occupation variable at each site: $\delta x_R = n_R - x$. Expanding the total energy in this configuration about the energy of the perfectly disordered state we get

$$E(x) = E^{(0)} + \sum_{R=1}^{N} E_R^{(1)} \delta x_R + \sum_{RR'=1}^{N} E_{RR'}^{(2)} \delta x_R \delta x_{R'} + \cdots . \tag{1}$$

The coefficients $E^{(0)}$, $E_R^{(1)} \ldots$ are the effective renormalized cluster interactions. $E^{(0)}$ is the energy of the averaged disordered medium. The renormalized pair interactions $E_{RR'}^{(2)}$ express the correlation between two sites and are the most dominant quantities for the analysis of phase stability. We will retain terms up to pair interactions in the configuration energy expansion. Higher-order interactions may be included for a more accurate and complete description. For the phase stability study it is the pair interaction which plays the dominant role.

The total energy of a solid may be separated into two terms: a one-electron band contribution E_{BS} and the electrostatic contribution E_{ES}. The renormalized cluster interactions defined in (1) should, in principle, include both E_{BS} and E_{ES} contributions. Since the renormalized cluster interactions involve the difference of cluster energies, it is usually assumed that the electrostatic terms cancel out and only the band structure contribution is important. Such an assumption, which is not rigorously true, has been shown to be approximately valid in a number of alloy systems [19]. Considering only the band structure contribution, the effective pair interactions may be written as

$$E_{RR'}^{(2)} = -\int_{-\infty}^{E_F} \mathrm{d}E \left\{ -\frac{1}{\pi} \operatorname{Im} \log \sum_{IJ} \det(G^{IJ}(E)) \xi_{IJ} \right\} \tag{2}$$

where G^{IJ} represents the configurationally averaged Green function corresponding to the disordered Hamiltonian whose R and R′ sites are occupied by Ith and Jth types of atom, and

$$\xi_{IJ} = \begin{cases} +1 & \text{if } I = J \\ -1 & \text{if } I \neq J. \end{cases}$$

The behaviour of this function is quite complicated and hence the integration by standard routines (e.g. Simpson's rule or Chebyshev polynomials) is difficult, involving many iterations before convergence is achieved. Furthermore the integrand is multi-valued, being simply the phase of $\sum_{IJ} \det(G^{IJ}) \xi_{IJ}$. The way out for this was suggested by Burke [11], which relies on the repeated application of the partition theorem on the Hamiltonian H^{IJ}. The final result is given simply in terms of the zeros and poles of the Green function in the region $E < E_F$:

$$E_{RR'}^{(2)} = 2 \sum_{IJ} \xi_{IJ} \sum_{k=0}^{\ell \max} \left[\sum_{j=1}^{z^{k,IJ}} Z_j^{k,IJ} - \sum_{j=1}^{p^{k,IJ}} P_j^{k,IJ} + (p^{k,IJ} - z^{k,IJ}) E_F \right] \tag{3}$$

where $Z_j^{k,IJ}$ and $P_j^{k,IJ}$ are the zeros and poles of the peeled Green function G_k^{IJ} of the disordered Hamiltonian with occupancy at sites R and R' by I and J of which the first $(k-1)$ rows and columns have been deleted. $p^{k,IJ}$ and $z^{k,IJ}$ are the number of poles and zeros in the energy region below E_F. The factor of 2 accounts for the spin degeneracy.

2.2. The augmented space recursion

As discussed in the previous section, the calculation of the effective pair interaction in our formalism reduces to the determination of the peeled configuration averaged Green functions $\langle G_k^{IJ}\rangle$. We shall employ the ASR coupled with the tight-binding linearized muffin tin orbital (TB-LMTO) method introduced by Andersen and Jepsen [20] for a first-principles determination of these configuration averaged quantities. We shall take the most localized, sparse tight binding first-order Hamiltonian derived systematically from the LMTO theory within the atomic sphere approximation (ASA) and generalized to random alloys. The ASR method has been described at great length in earlier papers [6–9, 12, 21, 22]. We refer the readers to these references for further details. We shall give here the final form of the effective Hamiltonian used for recursion in augmented space for the calculation of the peeled Green functions:

$$
\begin{aligned}
H_k^{IJ} = {} & \sum_{\ell=k}^{\ell\max} C_{R,\ell}^{I} a_R^{\dagger} a_R + \sum_{\ell=1}^{\ell\max} C_{R',\ell}^{J}\, a_{R'}^{\dagger} a_{R'} + \sum_{R''\neq R,R'} \sum_{\ell=1}^{\ell\max} (C_{R'',\ell}^{B} + \delta C_{\ell} \tilde{M}^{R''}) a_{R''}^{\dagger} a_{R''} + \cdots \\
& + \sum_{R''\neq R} \sum_{L=k} \sum_{L'} \Delta_{R,\ell}^{1/2,I} S_{LL'}^{R,R''} (\Delta_{R'',\ell'}^{1/2,B} + \delta\Delta_{\ell'}^{1/2} \tilde{M}^{R''}) a_R^{\dagger} a_{R''} + \cdots \\
& + \sum_{R''\neq R'} \sum_{L} \sum_{L'} \Delta_{R',\ell}^{1/2,I} S_{LL'}^{R',R''} (\Delta_{R'',\ell'}^{1/2,B} + \delta\Delta_{\ell'}^{1/2} \tilde{M}^{R''}) a_{R'}^{\dagger} a_{R''} + \cdots \\
& + \sum_{R''\neq R} \sum_{L} \sum_{L'=k} (\Delta_{R'',\ell}^{1/2,B} + \delta\Delta_{\ell}^{1/2} \tilde{M}^{R''}) S_{LL'}^{R'',R} \Delta_{R,\ell'}^{1/2,I}\, a_{R''}^{\dagger} a_R + \cdots \\
& + \sum_{R''\neq R'} \sum_{L} \sum_{L'} (\Delta_{R'',\ell}^{1/2,B} + \delta\Delta_{\ell}^{1/2} \tilde{M}^{R''}) S_{LL'}^{R'',R'} \Delta_{R',\ell'}^{1/2,I}\, a_{R''}^{\dagger} a_{R'} + \cdots \\
& + \sum_{R''\neq R,R'} \sum_{R'''\neq R,R'} \sum_{L} \sum_{L'} (\Delta_{R'',\ell}^{1/2,B} + \delta\Delta_{\ell}^{1/2} \tilde{M}^{R''}) S_{LL'}^{R'',R'''} \\
& \times (\Delta_{R''',\ell'}^{1/2,B} + \delta\Delta_{\ell'}^{1/2} \tilde{M}^{R'''}) (a_{R''}^{\dagger} a_{R'''} + a_{R'''}^{\dagger} a_{R''})
\end{aligned}
\tag{4}
$$

where L is a composite index (lm).

For a binary distribution $\tilde{M}^R$ is given by

$$
\tilde{M}^R = x\, b_{R\uparrow}^{\dagger} b_{R\uparrow} + (1-x)\, b_{R\downarrow}^{\dagger} b_{R\downarrow} + \sqrt{x(1-x)} (b_{R\uparrow}^{\dagger} b_{R\downarrow} + b_{R\downarrow}^{\dagger} b_{R\uparrow}). \tag{5}
$$

For non-isochoric alloys, the difference in atomic radii of the constituents leads to changes in the electronic density of states, as confirmed by experiment [23] and approximate theoretical techniques [24]. One thus expects that the mismatch of size produces, in addition to a relaxation energy E_R contribution, a change in the band structure. Within our ASR, off-diagonal disorder in the structure matrix S^{β}, because of local lattice distortions due to the size mismatch of the constituents, can be handled on the same footing as diagonal disorder in the potential parameters [22].

The ASR with the TB-LMTO Hamiltonian coupled with orbital peeling allows us to compute configuration averaged pair potentials directly, without resorting to any direct averaging over a finite number of configurations. In an earlier paper [7] we have discussed how one uses the local symmetries of the augmented space to reduce the Hamiltonian and carry

out the recursion on a reducible subspace of much lower rank. If we fix the occupation of two sites, the local symmetry of the augmented space is lowered (this is very similar to the lowering of spherical symmetry to cylindrical symmetry when a preferred direction is introduced in an isotropic system). We may then carry out the recursion in a suitably reduced subspace.

2.3. Static concentration wave method

The static concentration wave (SCW) was proposed as a theory for ordering by Khachaturyan [25, 26]. The occupation probability $n(\vec{r})$ plays the key role in this theory. This function $n(\vec{r})$ that determines the distribution of solute atoms in an ordered phase can be represented as a superposition of concentration waves:

$$n(\vec{r}) = c + \tfrac{1}{2}\sum_j [Q(\vec{k}_j)\exp(\mathrm{i}\vec{k}_j \cdot \vec{r}) + Q^*(\vec{k}_j)\exp(-\mathrm{i}\vec{k}_j \cdot \vec{r})] \tag{6}$$

where $\exp(\mathrm{i}\vec{k}_j \cdot \vec{r})$ is a SCW, $\vec{k}_j$ is a non-zero wavevector defined in the first Brillouin zone of the disordered alloy, $\vec{r}$ is a site vector of the lattice $\{\vec{r}\}$, the index j denotes the wavevectors in the Brillouin zone, $Q(\vec{k}_j)$ is the SCW amplitude and c is the atomic fraction of the alloying element.

The study of phase stability requires accurate approximations to the configurational energy as well as the use of statistical models to obtain the configurational entropy. The configurational energy within the pair interaction can be represented in Fourier space as the product of the Fourier transform of the effective pair interaction $V(\vec{k})$ and that of the pair correlation function $Q(\vec{k})$:

$$E \simeq \left(\frac{N}{2}\right)\sum_{\vec{k}} V(\vec{k})Q(\vec{k})$$

where N is the number of atoms. Minimization of E will naturally occur for states of order characterized by maxima in the $Q(\vec{k})$ pair correlation spectrum located in regions of the absolute minima of $V(\vec{k})$. Consequently, much can be predicted about the types of ordering to be expected from a study of the shape of $V(\vec{k})$, particularly from a search of its absolute minima (special points). At these points,

$$|\nabla_h V(h)| = 0.$$

This was pointed out by Lifshitz [27, 28] and Khachaturyan [25, 26]. Different types of ordered structures can be related directly to the minima of $V(\vec{k})$. In other words, given the knowledge of concentration wavevectors, one can readily predict the most stable ordered structure of the system at low temperatures. This is comparable to the knowledge derived from studies like those based on x-ray, electron and neutron diffraction. A peak at the Γ point, $\vec{k} = (000)$, indicates phase separation, while a peak at the Γ point, $\vec{k} = (100)$, in a fcc lattice suggests ordering. Peaks away from the special points may correspond to the formation of long period super-structures. Within a simple mean field approximation, the instability can be obtained in the following way: if we add the expression for the dominant quadratic term in the average energy to that of the configurational entropy under the simple mean field approximation we obtain an expression for the free energy:

$$F = \sum_{i,j} V_{ij}^2(n_i - c)(n_j - c) + k_B T \sum_i [n_i \ln n_i + (1 - n_i)\ln(1 - n_i)]$$

where n_i is the concentration of species A at the ith site and c is the average concentration of that species. If we define a configuration variable γ_i^0 as $\langle \delta n_i \rangle_0$ (the symbol $\langle \cdots \rangle_0$ denotes micro-

canonical averaging), which is the variable relevant to stability analysis, then the harmonic term in the Taylor expansion of the above free energy is

$$F^2 = \frac{N}{2}\sum_h \Gamma^*(\vec{k}(h))F(\vec{k}(h))\Gamma(\vec{k}(h)) \tag{7}$$

where $\vec{k}(h) = 2\pi h_\alpha \vec{b}_\alpha$ and $\Gamma(\vec{k}(h)) = \mathcal{F}(n(\vec{r}) - c)$. The stability of a solid solution with respect to a small concentration wave of a given wavevector $\vec{k}(h)$ is guaranteed as long as $F(\vec{k}(h))$ is positive definite. Instability sets in when $F(\vec{k}(h))$ vanishes, i.e.

$$F(\vec{k}(h)) = k_B T^i + V(\vec{k}(h))c(1-c) = 0 \tag{8}$$

T^i being the temperature at which the instability sets in for the concentration wave considered. It appears from the above expression that, under a simple mean field approximation, the spinoidal is always a parabola in the (t, c) phase diagram, symmetric about $x = 0.5$. It is the concentration dependence of the effective pair interactions which brings about the asymmetry.

3. Computational details

3.1. Convergence of augmented space recursion

The effective pair potentials are calculated at the Fermi level so one needs to be very careful about the convergence of the Fermi energy as well as that of the effective pair potentials. In fact, errors can arise in the ASR because one can carry out only a finite number of recursion steps and then terminate the continued fraction using available terminators. Also one chooses a large but finite part of the augmented space nearest-neighbour map and ignores the part of the augmented space very far from the starting state. This is also a source of error.

In order to determine the Fermi energy accurately, we have used the energy-dependent version of ASR. In this version of ASR the defining Hamiltonian is recast into an energy-dependent Hamiltonian having only diagonal disorder. We then choose a few seed points across the energy spectrum uniformly, carry out recursion on those points and spline fit the coefficients of recursion throughout the whole spectrum. This enables us to carry out a large number of recursion steps since the configuration space grows significantly less faster for diagonal, as compared with off-diagonal, disorder. For details see [29]

We have checked the convergence of the Fermi energy and effective pair potentials with respect to recursion steps and the number of seed energy points taking the case of the $NiPt_3$ system. We have found that the Fermi energy and effective pair potentials converge beyond 7 recursion steps and 35 seed energy points. All our calculations reported in the following have been carried out with 8 recursion steps and 35 seed energy points.

3.2. Anti-phase boundary energy

Kanamori and Kakehasi [30] used the method of geometrical inequalities which is capable of searching for ground structure. They considered the energy of the three-dimensional Ising-like model:

$$E_c = \sum_k V_k P_k \tag{9}$$

where V_k is the interaction constant of the kth nearest-neighbour interaction and P_k is the total number of kth neighbouring pairs in the given configuration. Defining the anti-phase boundary energy ξ by

$$\xi = -V_2 + 4V_3 - 4V_4, \tag{10}$$

Table 1. The special points and stars of the fcc structure.

$\boldsymbol{k}$-vector star	Members	BZ points	Ordering structure
$\langle 000\rangle$	[000]	Γ	
$\langle 100\rangle$	[100][010][001]	X	$L1_2$, $L1_0$
$\langle 1\frac{1}{2}0\rangle$	$[1\frac{1}{2}0][\frac{1}{2}01][01\frac{1}{2}]$	W	A_2B_2, DO_{22}
	$[\bar{1}\frac{\bar{1}}{2}0][\frac{\bar{1}}{2}0\bar{1}][0\bar{1}\frac{\bar{1}}{2}0]$		
$\langle\frac{1}{2}\frac{1}{2}\frac{1}{2}\rangle$	$[\frac{1}{2}\frac{1}{2}\frac{1}{2}][\frac{1}{2}\frac{\bar{1}}{2}\frac{\bar{1}}{2}]$	L	$L1_1$
	$[\frac{\bar{1}}{2}\frac{1}{2}\frac{\bar{1}}{2}][\frac{\bar{1}}{2}\frac{\bar{1}}{2}\frac{1}{2}]$		

the authors proved rigorously that, for $\xi > 0$, $L1_2$ and $L1_0$ are the corresponding super-structures possible at 25 and 50% concentration while for $\xi < 0$, one has the DO_{22} and A_2B_2 super-structures. We have applied these conditions in our calculations to find out the relative stability between DO_{22} and $L1_2$ structures in Ni_3Pt and $NiPt_3$ and those between A_2B_2 and $L1_0$ in NiPt.

3.3. Special-point ordering

A wide range of phenomena related to order–disorder and magnetic transitions can be explained using the symmetry properties of the pair potentials (V_{ij}). If a symmetry element (rotation, rotation–inversion or mirror plane) of the space group in $\boldsymbol{k}$ space is located at a point h, the vector representing the gradient $\nabla_h V(h)$ of an arbitrary potential energy function $V(h)$ at that point must lie along or within the symmetry element. If two or more symmetry elements intersect at point h, one must necessarily have

$$|\nabla_h V(h)| = 0 \tag{11}$$

since a finite magnitude vector cannot lie simultaneously on intersecting straight lines having only a point in common. At these so-called special points, the potential energy function $V(h)$ represents an extremum regardless of the choice of the pair interaction energies. Thus special points play an important role in the search for lowest energy ordered structures. The points which differ by a vector of a reciprocal lattice are considered equivalent. In the case of simple structures with a single atom per unit cell, it is sufficient that two symmetry elements intersect at special points. These special points are listed in crystallographic tables. They are always located at the surface of the Brillouin zone. The 'star' of a special point vector $\boldsymbol{k}$ is obtained by applying all the rotations and rotation–inversions of the space group on the vector $\boldsymbol{k}$. All these vectors of a star are also considered equivalent. The special points of the fcc structure are located at the points Γ, X, W and L of the Brillouin zone, as shown in table 1.

3.4. Ordering energy

The ordering energy is defined as the difference between the formation energy of an ordered alloy and the corresponding formation energy of a disordered alloy. Since we are dealing with the effective pair potentials, the ordering energy can be calculated using these pair potentials. The relation for ordering energy using pair potentials is given as

$$E^{ord} = \tfrac{1}{2}\sum_k V_k \delta x_o \delta x_k \tag{12}$$

where $\delta x_o\,(\delta x_k) = x_o\,(x_k) - x$, $x_o\,(x_k) = 1$ if the site o/k is occupied by an A atom and $x_o = 0$ if the site o/k is occupied by a B atom. For the $L1_2$ structure (for Ni_3Pt and $NiPt_3$ in our case)

Table 2. The calculated equilibrium lattice parameters with the choice of neutral charge spheres including scalar relativistic corrections. The corresponding lattice parameters without relativistic corrections are given in brackets.

Concentration of Pt	Equilibrium lattice parameter in au SR(NR)
0.00(Ni)	6.528(6.568) (expt 6.66)
0.25(Ni_3Pt)	6.758(6.890)
0.50(NiPt)	7.127(7.335)
0.75($NiPt_3$)	7.196(7.467)
1.00(Pt)	7.3685(7.683) (expt 7.41)

the expression for the ordering energy per atom in terms of pair potentials considering only up to fourth nearest neighbours is given as

$$E^{ord}_{Ni_3Pt} = -\tfrac{3}{32}[V_1 - \tfrac{1}{3}V_2 + V_3 - \tfrac{1}{3}V_4]. \tag{13}$$

For the $L1_0$ structure for NiPt the expression for the ordering energy per atom considering up to fourth nearest-neighbour pair potentials is given as

$$E^{ord}_{NiPt} = -\tfrac{1}{8}[V_1 - V_2 + V_3 - V_4]. \tag{14}$$

Using these two relations we have found the ordering energy for Ni_3Pt, NiPt and $NiPt_3$.

4. Results and discussions

We have applied our formalism discussed in the previous section in calculating the effective pair potentials for the fcc-based NiPt alloys for concentrations $x = 0.25, 0.5$ and 0.75 of Pt. The calculation of the effective pair potentials has been restricted up to fourth nearest-neighbour interactions. Total energy density functional calculations were performed at the concentrations $x = 0.25, 0.5$ and 0.75 of Pt. The Kohn–Sham equations were solved in the local density approximation (LDA). The LDA was treated within the context of LMTO in the ASA. The calculations were performed non-relativistically as well as scalar relativistically and the exchange correlation potential of Von Barth and Hedin was used. Two sets of calculations were performed: one with the same Wigner–Seitz radius (charged spheres) for Ni and Pt, and in the other set we followed the procedure described by Kudrnovský *et al* [18], using an extension of the procedure proposed by Andersen *et al* [20], which allows us flexibility in the choice of ASA radii for the constituents. The idea is to choose ASA radii of atomic species in such a way that the spheres are charge neutral on average. The potential parameters Δ_l^I and γ_l^I of the constituent I were then scaled by the factors $(s^I/s^{alloy})^{2l+1}$ to account for the fact that the Wigner–Seitz radius of constituent I, s^I, is different from that of the alloy, s^{alloy}. These potential parameters were used to parametrize the alloy Hamiltonian. For the purpose of ASR, seven shell maps were generated and 35 seed energy points recursion was performed, as explained in the previous section, to calculate the Fermi energy with the second-order LMTO–ASA Hamiltonian through the recursion method using eight levels of recursion and the analytical terminator of Luchini and Nex. For the effective pair potentials, we used the orbital peeling method within the framework of ASR for the calculation of the peeled averaged Green function described in detail in the earlier section.

In table 2, we have quoted the equilibrium lattice parameters that were used in our calculations. We obtained these by minimizing the total energies with respect to the lattice parameters. We have obtained slightly lower equilibrium lattice parameters as compared to the experimental ones. This is characteristic of the LDA, which overestimates bonding.

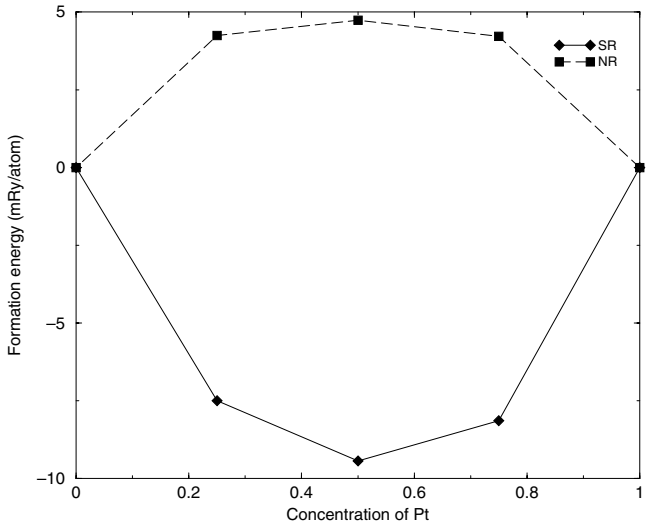

Figure 1. Formation energy versus concentration of Pt with the choice of neutral charge spheres.

Table 3. Formation energies for Ni_xPt_y with the choice of neutral charge spheres including scalar relativistic corrections. The values in brackets are without relativistic correction. The corresponding estimates for charged sphere calculations are shown with $*$'s. $**$ refers to calculations without combined corrections. $***$ refers to the disordered formation energy.

y	This work SR(NR)	Expt [31]	FPLMTO+ CWM [31]	LMTO [31]	LMTO+ CWM [32]	KKR-ASA (KKR-CPA)
0.25	−7.50(4.25)	−5.16	−6.30	−7.17	−6.66	
	−7.59*(4.17)*					
0.50	−9.44(4.74)	−7.06	−8.69	−8.5	−8.95	−12.00** [16]
	−9.02*(4.85)*					−8.10 [34]
						(−7.7***) [16]
0.75	−8.15(4.22)	−4.78	−6.40	−6.70	−9.12	
	−3.97*(6.65)*					

In figure 1 we have shown the formation energy of NiPt alloy systems with various Pt concentrations based on ordered calculations. It shows that, without the inclusion of relativistic effects, the formation energy comes out to be positive, which contradicts experimental results. With the inclusion of scalar relativistic corrections the formation energy comes out to be negative. This indicates that relativistic effects play an important role in the stability of NiPt alloys, in agreement with earlier studies. Our results are in closer agreement with previous works based on the full potential LMTO and the Connolly–Williams technique [31–33] and with experimental estimates. Singh *et al* [16] have also calculated the formation energy for 50% of Pt. Their results for the formation energy obtained from ordered calculations without combined corrections deviates quite a bit from ours as well as from other results based on the full potential LMTO and the Connolly–Williams technique [31–33], which is presumably due to the neglect of the combined correction in [16]. Singh *et al* [34] have also done the calculation with a combined correction, which shows better agreement. The full potential methods are expected to provide better estimates than other methods.

We next approached the problem from the disordered end. We started from a completely disordered alloy and set up concentration wave fluctuations in it to see when this destabilizes the

Table 4. The effective pair potentials for NiPt alloy systems calculated with potential parameters taken from calculations with the choice of charged spheres and including scalar relativistic correction. (O–L) refers to calculations without multipole corrections, *M* refers to calculations with multipole corrections and SCI to calculations with screened Coulomb interactions. US–PP refers to ultrasoft pseudo-potentials. ∗ refers to non-relativistic calculations.

Reference	v_1 (mRyd/atom)	v_2 (mRyd/atom)	v_3 (mRyd/atom)	v_4 (mRyd/atom)
	Concentration of Pt = 25%			
Present work	11.36	−0.05	−0.07	−0.41
	11.972∗	0.015∗	0.054∗	0.046∗
	Concentration of Pt = 50%			
Present work	7.832	0.114	−0.129	−0.057
	8.597∗	0.10∗	0.053∗	0.263∗
[16]	4.22	1.14	0.22	−1.04
	4.94*	0.52∗	0.32∗	−0.18∗
[14]	9.4∗	0.8∗	0.4∗	−0.2∗
[38]				
CWM–ASA + M	5.00	0.25	0.19	−0.28
SGPM	5.28	0.06	−0.82	−0.66
[17]				
with SGPM				
ASA + M(O–L)(SCI)	14.05(15.44)	0.32(−0.10)	−1.09(−1.22)	−1.76(−0.84)
ASA (SCI)	12.26(14.35)	0.53(−0.15)	−1.31(−1.48)	−2.14(−0.98)
With Connolly–Williams				
ASA + M	12.68	1.31	−0.02	−0.73
ASA + M(O–L)	13.70	0.49	−0.86	−1.39
ASA	14.33	0.28	−1.72	−1.92
US(PP)	12.81	1.30	0.69	−0.40
Direct calculation (SCI)				
ASA + M	12.45	0.47	−0.49	−0.65
	Concentration of Pt = 75%			
Present work	2.785	0.236	−0.116	0.276
	3.813∗	0.361∗	−0.175∗	0.366∗

disordered phase, as suggested by Khachaturyan [25]. The calculation of the lattice distortion for disordered alloys has been carried out within the structural model given by the rigid ion structure (RIS) [35]. According to this model the lattice relaxes in such a way as to keep all the nearest-neighbour distances close to the sum of the corresponding atomic radii for a particular concentration. This is found to be a reasonable model to deal with lattice relaxation effects in non-isochoric alloys [10]. Due to the distortion of the lattice, the structure matrix $S_{LL'}^{RR'}$ (which is a 9×9 matrix for each RR' pair and a spd basis set) can randomly take values $S_{LL'}^{AA}$, $S_{LL'}^{BB}$ and $S_{LL'}^{AB}$, depending upon the occupying of sites R and R':

$$S_{LL'}^{RR'} = S_{LL'}^{AA} n_R n_{R'} + S_{LL'}^{AB}[n_R(1 - n_{R'}) + (1 - n_R)n_{R'}] + S_{LL'}^{BB}(1 - n_R)(1 - n_{R'})$$

where

$$n_R = \begin{cases} 1 & \text{if } R \text{ is occupied by A} \\ 0 & \text{if } R \text{ is occupied by B.} \end{cases}$$

Considering the example of the calculation of $S_{LL'}^{AB}$, where B is the larger atom (e.g. Pt in the present case), this matrix for a specific pair among 12 nearest neighbours connects an A

Table 5. The effective pair potentials for NiPt alloys with potential parameters taken from calculations with the choice of charge neutral spheres including scalar relativistic corrections. The corresponding estimate for non relativistic calculations are shown with ∗'s.

Reference	v_1 (mRyd/atom)	v_2 (mRyd/atom)	v_3 (mRyd/atom)	v_4 (mRyd/atom)
		Concentration of Pt = 25%		
Present work	12.34	−0.092	−0.046	−0.54
	13.08∗	−0.021∗	0.152∗	−0.041∗
		Concentration of Pt = 50%		
Present work	10.08	0.1	0.004	−0.24
	10.111∗	0.126∗	0.246∗	0.175∗
[16]	16.02	1.34	0.06	−1.58
	11.96∗	0.66∗	0.28∗	−0.46∗
[17]				
Neutral (GPM)	5.49	1.22	0.01	−0.73
		Concentration of Pt = 75%		
Present work	8.9	0.26	0.1	0.02
	7.874∗	0.297∗	0.276∗	0.34∗

atom at the site (0, 0, 0) and a B atom, which in the undistorted case would have been at the position $(\frac{a}{2}, \frac{a}{2}, 0)$ and is now at $((\frac{a}{2} + d), (\frac{a}{2} + d), d)$, where d is the displacement due to lattice distortion and a is the lattice constant. We have assumed that the lattice expands equally in the x, y and z directions. With these new coordinates and assuming that all other neighbouring coordinates are fixed at undistorted fcc positions (which is the essence of the terminal point approximation [18]), we have computed the structure matrices $S^{AA}_{LL'}$, $S^{AB}_{LL'}$ and $S^{BB}_{LL'}$. This takes into account both the effect of radial distortion as well as angular distortion (the nearest neighbour is now $\sqrt{\frac{a^2}{2} + 2ad + 3d^2}$ instead of $\frac{a}{\sqrt{2}}$ and the nearest-neighbour vector is $((\frac{a}{2}+d), (\frac{a}{2}+d), d)$ instead of $(\frac{a}{2}, \frac{a}{2}, 0)$ in the above example). The values of d for $S^{AB}_{LL'}$ came out to be 0.064, 0.052 and 0.054 a for 25, 50 and 75% concentration of Pt. The details of the calculation scheme can be found in [10]. In figure 2 we have shown the relative magnitudes of the nearest-neighbour distances for different concentrations of Pt in NiPt alloy systems compared to values for the average bond length due to Vegard's law. We have computed the effective pair potentials for two sets of potential parameters with charged and charge neutral spheres. Figure 3 shows that the effective pair potentials for $NiPt_3$ is very small in magnitude using potential parameters with charged spheres. We even used these pair potentials and calculated the anti-phase boundary energy according to the prescription described in the previous section. The anti-phase boundary energy comes out to be negative for $NiPt_3$ and NiPt, indicating the stability of DO_{22} over $L1_2$ for $NiPt_3$ and A_2B_2 over $L1_0$ for NiPt. Further we calculated the minima of the special points according to the prescription described in the previous section. In the case of $NiPt_3$ and NiPt shown in figure 5, we could not get the minima at $\langle 100 \rangle$, which is not quite correct because experiments show that $NiPt_3$ has $L1_2$ and NiPt has $L1_0$ ordering. But in the case of Ni_3Pt we could get the positive anti-phase boundary energy as well as the minima at $\langle 100 \rangle$, correctly showing the ordering $L1_2$. In figure 4 we have plotted the effective pair potentials as a function of energy relative to the Fermi energy and number of neighbouring shells with charge neutral potential parameters including scalar relativistic corrections, which shows that the first nearest-neighbour pair potentials are larger in magnitude than the second, third and fourth nearest-neighbour pair potentials. With potential

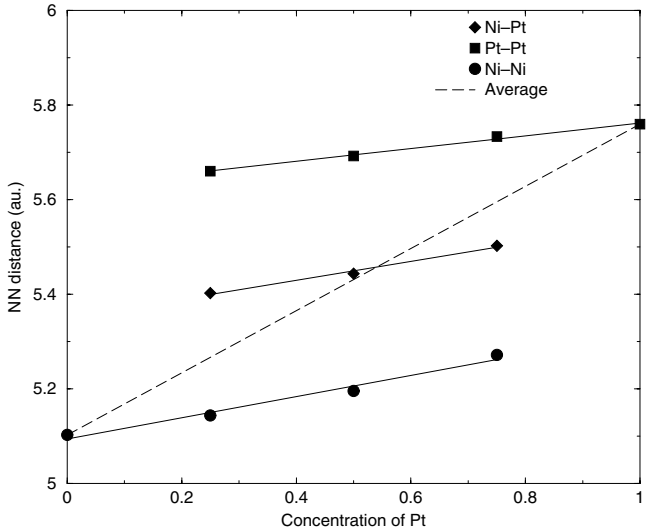

Figure 2. Nearest-neighbour distance versus concentration of Pt with the choice of neutral charge spheres. For comparison the average bond length given by Vegard's law is shown by a broken line.

Table 6. The anti-phase boundary energies for Ni_xPt_y alloys from charged and neutral sphere calculations.

	APB energy (mRyd/atom)	
	Charged spheres	Neutral spheres
Concentration of Pt	Relativistic (non-relativistic)	
0.25	1.41(0.017)	2.07(0.793)
0.50	−0.402(−0.94)	0.876(0.158)
0.75	−1.804(−2.525)	0.06(−0.553)

parameters from neutral sphere calculations including scalar relativistic corrections for $NiPt_3$ and NiPt the anti-phase boundary energies come out to be positive and the minima of special points are at $\langle 100 \rangle$, correctly showing $L1_2$ and $L1_0$ orderings. If we use charge neutral potential parameters without including scalar relativistic effects the anti-phase boundary energies come out to be positive for Ni_3Pt and NiPt but negative for $NiPt_3$. This shows that, for $NiPt_3$, both scalar relativistic as well as charge transfer effects play an important role in predicting the correct ground state.

So, we argue that, on increasing the concentration of Pt atoms, the careful treatment to take into account the charge transfer effect becomes increasingly important. In figure 4, we have also shown the effective pair potentials without scalar relativistic corrections. For $NiPt_3$ it is clearly seen that the effective pair potentials with scalar relativistic corrections are larger in magnitude than the non-relativistic ones, which is expected because of the higher concentration of Pt.

In figure 6 we have plotted the effective pair potentials versus concentration of Pt with charge neutral potential parameters including scalar relativistic corrections, which show that the first nearest-neighbour effective pair potentials decrease with an increase of the Pt concentration. Singh *et al* [16, 36] have also calculated the effective pair potentials

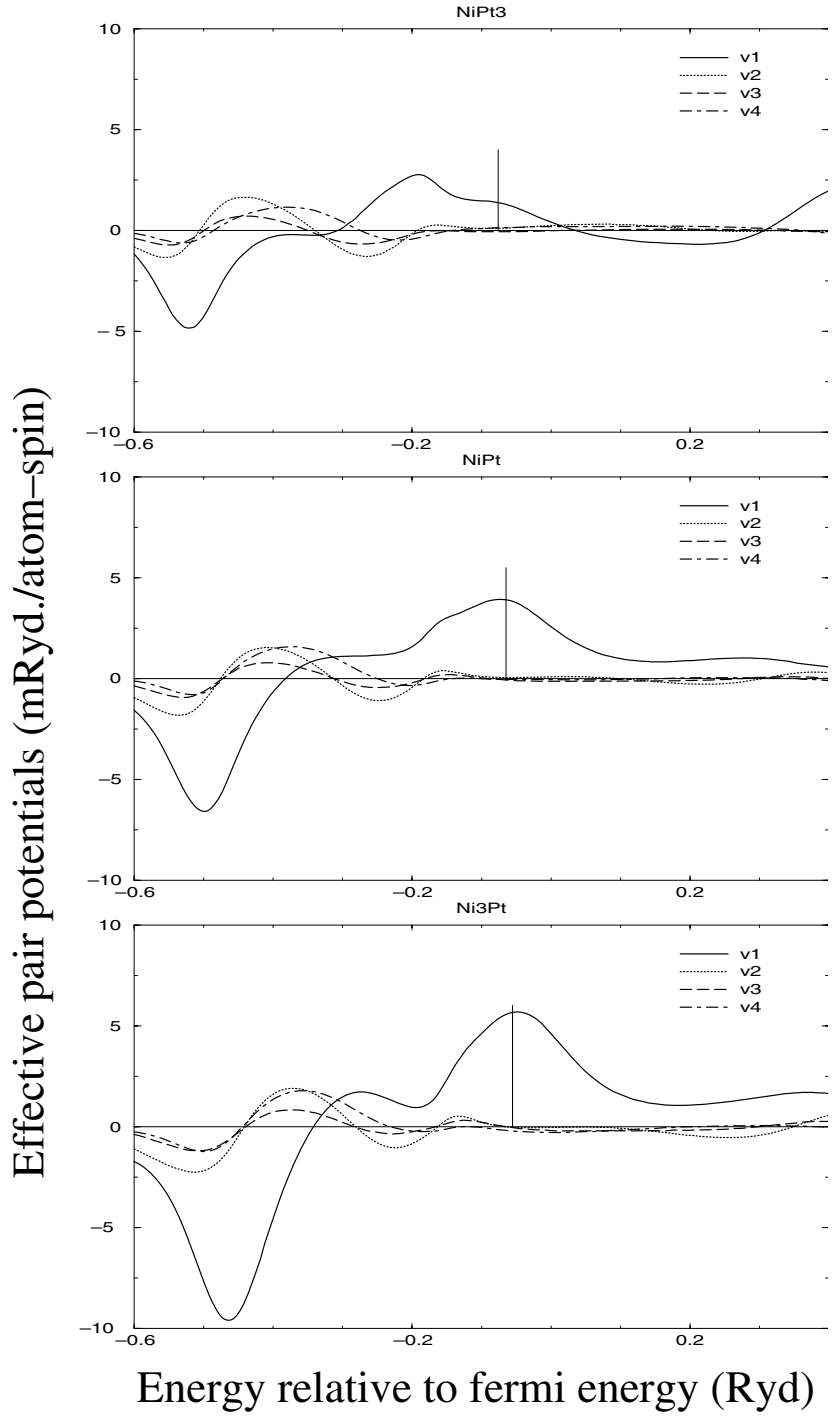

Figure 3. The effective pair potentials with potential parameters taken from calculations with the choice of charged spheres including scalar relativistic corrections.

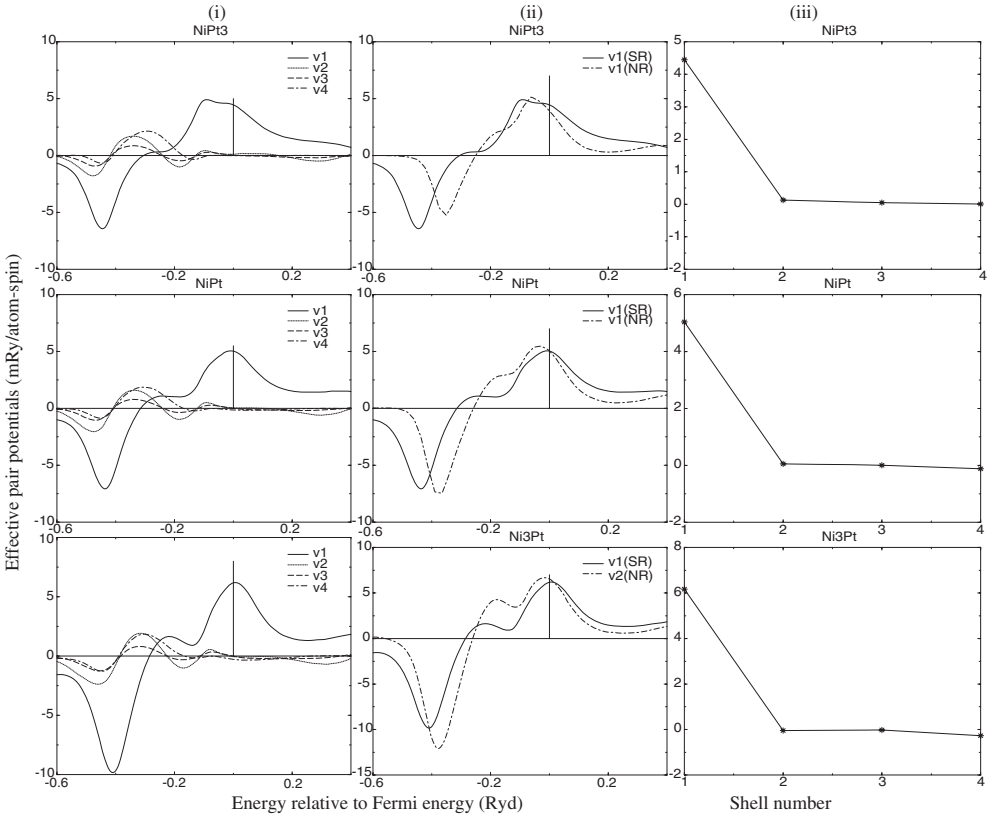

Figure 4. (i) The effective pair potentials as a function of energy relative to the Fermi energy with charge neutral potential parameters including scalar relativistic corrections. (ii) Comparison between the first nearest-neighbour effective pair potentials with scalar relativistic corrections and without scalar relativistic corrections by taking charge neutral potential parameters. (iii) The effective pair potentials as a function of shell numbers with charge neutral potential parameters including scalar relativistic correction.

using the KKR-CPA-GPM method. Their values of effective pair potentials are much larger than ours. They pointed out that, due to the large values of effective pair potentials, the ordering energy and ordering temperatures (transition temperatures) are much higher than those observed experimentally. Our estimates give rise to instability temperatures which are closer to the experimental results (shown in figure 7). For example, our estimate for the instability temperature for the 50% alloy is 1683 K, whereas the estimate from the KKR-CPA is around 2979 K. The experimental estimate of the transition temperature is 950 K [37]. In the KKR-CPA-GPM method one considers only the single-site approximation and one does not take into account any off-diagonal disorder which may arise because of size mismatch of the constituent atoms. The ASR, on the other hand, as discussed earlier can do this with facility. Our test calculation for NiPt (50% concentration of Pt) without taking into account lattice relaxation due to the size mismatch effect gives an estimate of the instability temperature of 2363 K, which is indeed higher than that of our original estimate taking into account lattice relaxation due to the size mismatch effect. Furthermore, Singh *et al* [16, 36] in their calculation for charge neutrality have taken the ratio of Wigner–Seitz radii of Ni and Pt as 0.95. We, on the other hand, have varied the ratio, with the provision that the total volume is conserved,

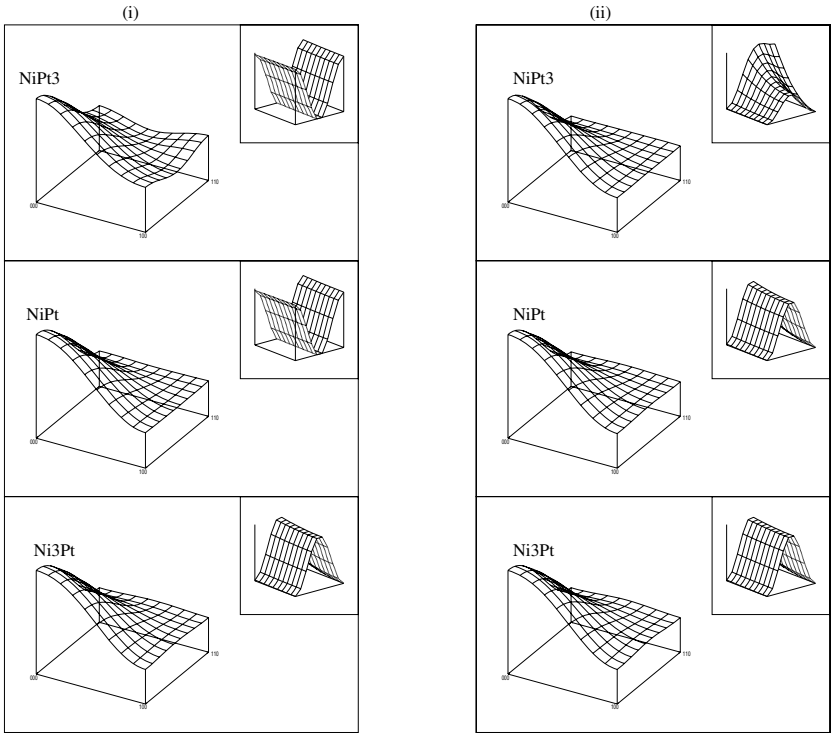

Figure 5. The $V(\vec{k})$ surface for NiPt alloy systems with potential parameters calculated with the choice of (i) charged spheres and (ii) charge neutral spheres on the $k_z = 0$ plane. The figures in the inset are the corresponding rescaled $V(\vec{k})$ surfaces on the $k_z = 0$ plane along the (100) to (110) direction to view the minima.

until, on average, the spheres become charge neutral. We have observed the ratio to be 0.909, 0.913 and 0.919 for the Ni_3Pt, NiPt and $NiPt_3$. Given these calculational differences, it is not surprising that our calculations result in smaller values of the pair potentials, leading to better estimates of the instability temperatures. The calculations of Pinski *et al* [14] were carried out without scalar relativistic effects. Their values are consequently rather large compared to ours. Ruban *et al* [17] have calculated pair potentials for 50% concentration of Pt using different methods and showed that different methods give different values of pair potentials. Their nearest-neighbour pair potential is slightly higher than ours. The effective pair potentials obtained by Pourovskii *et al* [38] from the neutral charge sphere GPM method are similar to the estimates of Ruban *et al* [17].

In figure 7 we have shown the ordering energy, anti-phase boundary energy and instability temperatures versus concentration of Pt with charge neutral potential parameters including scalar relativistic corrections. The ordering energy in all three cases Ni_3Pt, NiPt and $NiPt_3$ is negative, showing the stability of the ordered structures compared to the disordered solution. Among all three concentrations, NiPt attains the maximum value of ordering energy, which confirms that $L1_0$ in NiPt systems is the most stable structure. The anti-phase boundary energy in all these cases Ni_3Pt, NiPt and $NiPt_3$ comes out to be positive, showing the ordering structures $L1_2$ for Ni_3Pt, $L1_0$ for NiPt and $L1_2$ for $NiPt_3$, as described above. The magnitude of the instability temperatures using the charge neutral potential parameters comes out to be larger than the experimental transition temperatures. However, the qualitative trend of the change of

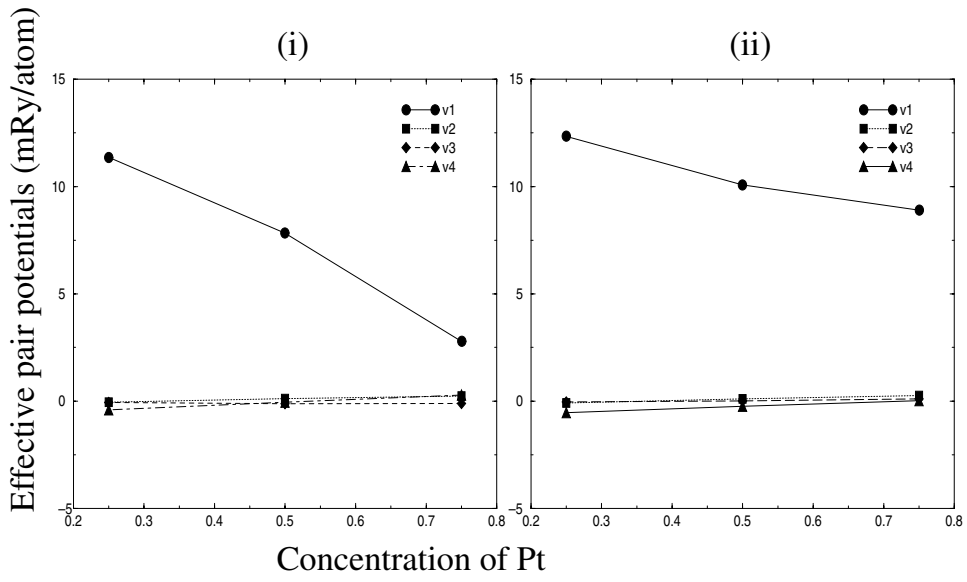

Figure 6. The effective pair potentials versus concentration of Pt with the choice of potential parameters with (i) charged spheres including scalar relativistic correction and (ii) charge neutral spheres including scalar relativistic corrections.

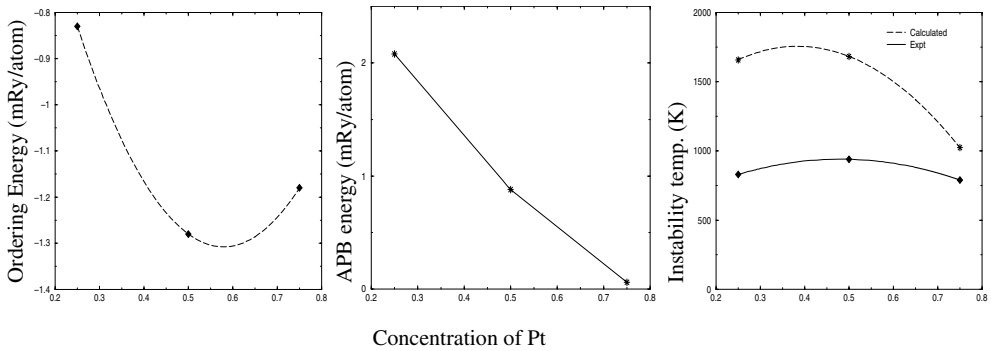

Figure 7. Ordering energy, anti-phase boundary energy and instability temperatures versus concentration of Pt with the choice of charge neutral potential parameters including scalar relativistic corrections.

instability temperatures with changing concentration of Pt is correct. The calculated qualitative phase diagram (instability temperature versus concentration of Pt) shows an asymmetric feature which is not observed experimentally. This could be due to the neglect of magnetism in the calculations of effective pair interactions, which can have a significant effect particularly at the high concentrations of Ni. Amador *et al* [31] also reported the phase diagram (instability temperature versus concentration of Pt) of this system described by the nearest-neighbour tetrahedron effective interactions from clusters with appropriate effective volume. Their values for transition temperatures are smaller than ours but there is high asymmetry in their phase diagram and even the trend is not the same as found in experiments.

5. Conclusion

Our total energy calculations for the ordered alloys indicate that, in order to have the correct sign for the formation energy, it is essential to include relativistic corrections. Our analysis of the concentration wave approach indicates that, for Ni_3Pt, neither relativistic corrections nor the charge transfer effect is essential for the correct prediction of the $L1_2$ ground state. For NiPt, although scalar relativistic corrections are not essential, careful treatment of the charge transfer effect is a must to predict the correct ground state ($L1_0$). For $NiPt_3$ both these corrections are essential to predict the correct ground state $L1_2$.

Although it seems that qualitatively the relativistic corrections and charge transfer effect play the essential role only for high Pt content alloys, for quantitative prediction of the instability temperature both these corrections are required across the concentration range.

The main conclusions of this paper are:

- We have demonstrated that for accurate prediction of the ground state structures and instability temperatures for alloys with components with large atomic size differences, like NiPt, it is essential to take into account both relativistic corrections and the averaged charge neutrality of the atomic spheres.
- We have also demonstrated that ASR combined with the first-principles TB-LMTOs and orbital peeling are both computationally feasible and suitable techniques for such studies are described above.

These techniques will form the basis of our further studies into similar alloy systems, but with magnetic effects included.

References

[1] Gonis A, Zhang X G, Freeman A J, Turchi P, Stocks G M and Nicholson D M 1987 *Phys. Rev.* B **36** 4630
[2] Connolly J W D and Williams A R 1983 *Phys. Rev.* B **27** 5169
[3] Ducastelle F and Gautier F 1976 *J. Phys. F: Met. Phys.* **6** 2039
[4] Gonis A and Garland J W 1977 *Phys. Rev.* B **16** 2424
[5] Dreyssé H, Berera A, Wills L T and de Fontaine D 1989 *Phys. Rev.* B **39** 2442
Wolverton C, Ceder G, de Fontaine D and Dreyssé H 1993 *Phys. Rev.* B **48** 726
[6] Saha T, Dasgupta I and Mookerjee A 1995 *J. Phys.: Condens. Matter* **6** L245
Saha T and Mookerjee A 1996 *J. Phys.: Condens. Matter* **8** 2915
Dasgupta I, Saha T and Mookerjee A 1993 *Phys. Rev.* B **51** 17724
[7] Saha T, Dasgupta I and Mookerjee A 1994 *J. Phys.: Condens. Matter* **6** L245
[8] Haydock R, Heine V and Kelly M J 1972 *J. Phys. C: Solid State Phys.* C **5** 2845
Haydock R 1988 *Solid State Physics* vol 35 (New York: Academic)
[9] Ghosh S, Das N and Mookerjee A 1999 *J. Phys.: Condens. Matter* **9** 10701
Chakrabarti A and Mookerjee A 2001 *J. Phys.: Condens. Matter* **13** 10149
[10] Saha T and Mookerjee A 1996 *J. Phys.: Condens. Matter* **8** 2915
[11] Burke N R 1976 *Surf. Sci.* **58** 349
[12] Saha T 1995 *PhD Thesis* Jadavpur University
[13] Treglia G and Ducastelle F 1987 *J. Phys. F: Met. Phys.* **17** 1935
[14] Pinski F J, Ginatempo B, Johnson D D, Staunton J B, Stocks J M and Györffy B L 1991 *Phys. Rev. Lett.* **66** 776
Pinski F J, Ginatempo B, Johnson D D, Staunton J B, Stocks J M and Györffy B L 1992 *Phys. Rev. Lett.* **68** 1962
[15] Lu Z W, Wei S H, Wei and Zunger A 1991 *Phys. Rev. Lett.* **66** 1753
Lu Z W, Wei S H, Wei and Zunger A 1992 *Phys. Rev. Lett.* **68** 1961
[16] Singh P P, Gonis A and Turchi P A E 1993 *Phys. Rev. Lett.* **71** 1605
[17] Ruban A V, Simak S I, Korzhavyi P A and Skriver H L 2002 *Phys. Rev.* B **66** 024202
[18] Kudrnovský J and Drchal V 1990 *Phys. Rev.* B **41** 7515
[19] Heine V 1988 *Solid State Physics* vol 35 (New York: Academic)

[20] Andersen O K and Jepsen O 1984 *Phys. Rev. Lett.* **53** 2571
[21] Mookerjee A 1973 *J. Phys. C: Solid State Phys.* C **6** 1340
[22] Saha T, Dasgupta I and Mookerjee A 1995 *Phys. Rev.* B **51** 3413
[23] Wright H, Weightman P, Andrews P T, Folkerts W, Flipse C F J, Sawatsky G A, Norman D and Padmore H 1987 *Phys. Rev.* B **35** 519
[24] Bose S K, Kudrnovský J, Jepsen O and Andersen O K 1992 *Phys. Rev.* B **45** 8272
[25] Khachaturyan A G 1978 *Prog. Mater. Sci.* **22** 1
[26] Khachaturyan A G 1983 *Theory of Structural Transformations in Solids* (New York: Wiley)
[27] Landau L D and Lifshitz E M 1969/1980 *Statistical Physics* 2nd and 3rd edn, part 1 (Oxford: Pergamon)
[28] Krivoglaz M A and Smirnov A A 1964 *The Theory of Order–Disorder in Alloys* (London: McDonald)
[29] Ghosh S D 2000 *PhD Thesis* Jadavpur University
[30] Kanamori J and Kakehasi Y 1977 *J. Physique Coll.* **38** C7 274
[31] Amador C, Lambrecht W R L, van Schilfgaarde M and Segall B 1993 *Phys. Rev.* B **47** 15276
[32] Ruban A V, Abrikosov I A and Skriver H L 1995 *Phys. Rev.* B **51** 12958
[33] de Fontaine D 1994 *Solid State Physics* vol 47, ed H Ehrenreich, F Seitz and D Turnbull (New York: Academic) p 33
[34] Singh P P and Gonis A 1994 *Phys. Rev.* B **49** 1642
[35] Maŝek J and Kudrnovský J 1986 *Solid State Commun.* **58** 67
[36] Singh P P 1996 *Pramana* **47** 99
[37] Dahmani C E, Cadeville M C, Sanchez J M and Moran-Lopez J L 1985 *Phys. Rev. Lett.* **55** 1208
[38] Pourovskii L V, Ruban A V, Abrikosov I A, Vekilov Y Kh and Johansson 2001 *Phys. Rev.* B **64** 035421